TECHNICAL REPORT No. 61

EMPIRICAL ORTHOGONAL FUNCTION ANALYSIS OF THE ZONAL AND EDDY COMPONENTS OF 500mb HEIGHT FIELDS IN THE NORTHERN EXTRATROPICS

by

Franco Molteni*

* This work was carried out while the author was a Visiting Scientist at ECMWF, on leave from:
C.N.R.- Istituto di Cosmo-Geofisica, Torino, Italy

February 1987

ABSTRACT

In this study empirical orthogonal functions (EOFs) are computed separately from the zonally-averaged and the eddy components of 500 mb height fields in the Northern Hemisphere extratropics. The data sample includes 1152 5-day-mean fields covering 32 cold seasons (October-March) and is derived from NMC and ECMWF analyses. The variance of the coefficients of the most relevant EOFs are analysed, separating the contributions of seasonal cycle and interannual variability.

The first eddy EOF is representative of the wintertime stationary eddies, the following ones show many similarities with teleconnection patterns already revealed in previous observational studies of the low-frequency variability of the atmosphere. The 2nd and the 4th eddy EOF also resemble barotropically unstable linear modes of the wintertime circulation, and a significant proportion of their variance is due to interannual variability.

The first 3 zonal EOFs are representative of the mean westerly flow, of the latitudinal position of the jet maximum and of the split of the jet, respectively. The zonal coefficients 1 and 2 are also significantly influenced by the interannual variability and show the greatest anomaly autocorrelation among all the zonal and eddy EOF coefficients at lags of 10-15 days.

CONTENTS Page No.

1. INTRODUCTION 1

2. DATA SET AND ANALYSIS PROCEDURES 3

3. EVALUATION OF THE SEASONAL CYCLE AND THE INTERANNUAL VARIABILITY OF THE EOF COEFFICIENTS 8

4. THE EOFs OF THE EDDIES 12

5. THE EOFs OF THE ZONAL MEANS 22

6. SUMMARY AND CONCLUSIONS 27

ACKNOWLEDGEMENTS 28

REFERENCES 29

APPENDIX 1 A1.1

APPENDIX 2 A2.1

1. INTRODUCTION

Empirical orthogonal function (EOF) analysis has been widely used in observational studies to determine the spatial patterns associated with the most important modes of variation of meteorological and climatological variables. EOFs are usually determined as eigenvectors of a dispersion matrix, whose elements are the covariances (sometimes the correlations) between the time series of a variable observed in a number of contiguous locations. The time series of the EOF coefficients (that is, the projections of each instantaneous field onto the EOFs) have the property that, for each possible truncation of the EOF series, the subspace generated by the first n coefficients explains the greatest proportion of variance of the observed data set among all the linear subspaces of the same dimension.

The physical significance of the EOFs has often been questioned; Buell (1975, 1979) demonstrated that, if the covariance structure of the analyzed field is uniform and isotropic, the spatial features of the EOFs are strongly determined by the shape of the boundaries of the spatial domain. So, a realistic correspondence between the EOF patterns and the actual modes of variation exists only if the spatial boundaries are located in areas with low variability in the observed field, and the EOF patterns differ from obvious wave-like structures only if significant anisotropies occur in the variance-covariance distribution. Of course, even if these conditions are satisfied, the identification of the physical processes that are responsible for these modes of variation remains an open problem.

The field of geopotential height at 500 mb over the northern extratropics is ideal for an EOF analysis for a number of reasons. First of all, records of this field are now available for at least three decades with reasonable accuracy and resolution; the border of this area, i.e. the northern subtropical band, is in fact a region of low variability for the geopotential field; in addition, we know from a number of observational studies that the covariance structure characteristic of low-frequency variability of the atmosphere is far from isotropic, as can be seen, for example, from the teleconnection patterns identified by Wallace and Gutzler (1981).

EOF analyses of the 500 mb height in the northern extratropics were performed, among others, by Rinne and Karhila (1979) using a very large set of instantaneous fields covering all the seasons of the year, and by Wallace and

Gutzler (1981; hereafter referred to as WG) using monthly means in the winter season. In general, the subtraction of a mean value from each data series implies that the EOFs are representative of the anomalies of the field with respect to a time-averaged state. On the other hand, in many theoretical or diagnostic works on the large-scale circulation the dynamical fields have been decomposed into a zonally-symmetric and an eddy component, and this different approach has prevented an easy comparison between these studies and results of EOF analyses.

In this study, which is limited to the 'cold' season from October to March and uses a data sample including 32 years of analyses, EOFs have been computed separately from the zonally-averaged and the eddy fields of 500 mb height from 20°N to 90°N, without subtracting a time-mean field. The aim of this procedure is to give evidence to some modes of atmospheric variability, such as the variations in the mean zonal gradient or in the amplitude of the stationary waves, that have received plenty of attention in theoretical studies but are difficult to isolate when the traditional, anomaly-based EOF approach is adopted.

2. DATA SET AND ANALYSIS PROCEDURES

In this study we consider 500 mb geopotential heights over the Northern hemisphere starting from October 1952 to March 1984. From the beginning of our sample to December 1979 the data are derived from a wider data set (beginning in January 1946 and covering all the seasons of the year) available at the European Centre for Medium Range Weather Forecast (ECMWF). This set is based on operational analyses of the U.S. National Meteorological Center (NMC), and it was prepared under a WMO project that resulted in the publication of a four-volume report in the WMO long-range forecasting research publication series (Wallace, et al., 1983). In our study, we avoided the use of the first six years available in the original catalog, since a preliminary investigation showed that the quality of these first analyses was not adequate for our purposes. We added data from January 1980 to March 1984 derived from operational ECMWF analyses.

The NMC data were originally available over an octagonal, polar sterographic grid with a 381 km grid mesh, covering the whole Northern extratropics north of 20°N. The ECMWF analyses, archived as spherical harmonic coefficients, were retrieved on a 5° regular latitude-longitude grid (LLG). Neither of these two grids were suitable for our study; the former does not allow an easy computation of the zonal means and the latter has the disadvantage that the area represented by each grid point decreases proportionally to the cosine of latitude: an EOF analysis using this second grid would give an excessive weight to the variability in the polar area. Hence, all the data were interpolated onto a new LLG for which the number of points in each constant latitude line is proportional to the cosine of latitude. The parameters of the new grid were chosen in a way to obtain the same resolution as in a regular 5° LLG at the equator.

More precisely, if λ and ϕ indicate longitude and latitude, respectively, our grid can be defined as the ensemble of the points

$$\underline{x}_k = (\lambda_i, \phi_j)$$

where

$$j = 1, \ldots, 15 \qquad \phi_j = 90° - (j-1) \times 5°$$

$$i = 1, \ldots, N_j \qquad \lambda_i = (i-1) \times 360°/N_j$$

$$N_j = 1 \text{ for } j = 1$$

$$= \text{nearest integer to } (72 \cos \phi_j) \text{ for } j>1$$

$$k = i + \sum_{1}^{j-1} {}_{\ell}\, N_{\ell} = 1, \ldots, N$$

$$N = \sum_{j}^{15} {}_{j}\, N_{j} = 577$$

Finally, due to data availability and to avoid excessive computational burden, we consider only mean pentads (i.e., five-day, non-overlapping means) in the periods October through March. Over all we have considered 1152 pentads. Each cold season (i.e., October through March) includes 36 pentads, and the data set contains 32 cold seasons. The first pentad of each season is defined as the interval from 3 to 7 October (inclusive) of each year, the last one as the period from 27 to 31 March. In the following, we shall refer to October as to the period including the first six pentads, to November as to the pentads 7 to 12, etc.; we shall also use the term "year 1953" to indicate the cold season October 1952 through March 1953, and so on.

Let $z_p(\lambda_i, \phi_j)$ be the value of 500-mb height over the point $\underline{x}_k$, in pentad p, (p=1, ...1152). For each pentad field, we computed the following quantities:

- The northern extratropical mean:

$$z_o = \frac{1}{N} \sum_{1}^{15} {}_{j} \sum_{1}^{N_j} {}_{i}\, z_p(\lambda_i, \phi_j) \qquad (1a)$$

- The zonal means:

$$\bar{z}_p(\phi_j) = \frac{1}{N_j} \sum_{1}^{N_j} {}_{i}\, z_p(\lambda_i, \phi_j) \qquad (1b)$$

- The zonal mean departures from z_o:

$$\hat{z}_p(\phi_j) = \bar{z}_p(\phi_j) - z_o \qquad (1c)$$

- The eddy field:

$$z^*_p(\lambda_i,\phi_j) = z_p(\lambda_i,\phi_j) - \bar{z}(\phi_j). \tag{1d}$$

An NxN cross product matrix H* for the eddy component was defined as follows:

$$H^*_{k\ell} = \frac{1}{1152} \sum_{1}^{1152}{}_p \; z^*_p(\underline{x}_k)\; z^*_p(\underline{x}_\ell) \tag{2}$$

and the EOFs for the eddies were computed as the eigenvectors $\underline{e}^*_m$ of H*, m=1, ..., N. These EOFs were scaled so that their root mean square (rms) value over the grid was 1; if δ_{nm} is Kronecker's delta, we can write

$$\langle \underline{e}^*_m \; \underline{e}^*_n \rangle = \frac{1}{N} \sum_{1}^{N}{}_k \; e^*_m(\underline{x}_k)\; e^*_n(\underline{x}_k) = \delta_{mn} \tag{3}$$

where the operator <> defines the expectation value over our grid. This slightly non-standard normalisation has the advantage that the elements of the eigenvectors have order of magnitude 1 rather than $1/\sqrt{N}$.

The time coefficients representing the projections of each eddy field on the EOFs are defined by

$$C^*_{mp} = \langle \underline{e}^*_m \; \underline{z}^*_p \rangle = \frac{1}{N} \sum_{1}^{N}{}_k \; e^*_m(\underline{x}_k)\; z^*_p(\underline{x}_k) \tag{4}$$

They are orthogonal in time, and their mean square value is proportional to the eigenvalue associated with the corresponding EOF:

$$\frac{1}{1152} \sum_{1}^{1152}{}_p \; C^*_{mp}\; C^*_{np} = \delta_{mn}\; V^*_m = \delta_{mn}\; \frac{L^*_m}{N} \tag{5}$$

where

$$H^*\; \underline{e}^*_m = L^*_m\; \underline{e}^*_m. \tag{6}$$

The EOFs of the zonal means were computed in a way that assures coherence with the analysis of the eddy part. The zonal departures $\hat{\underline{z}}_p$ were used for the

analysis: in this way, the zonal EOFs are representative of zonal gradients of geopotential height, and the associated coefficients give indications on the intensity and the latitudinal distribution of the mean zonal wind.

The technique described in Appendix 1 allowed the definition of a set of zonal EOFs $\hat{\underline{e}}_m$ and time coefficients $\hat{C}_{mp}$ with the following properties:

$$\langle \hat{\underline{e}}_m \hat{\underline{e}}_n \rangle = \frac{1}{N} \sum_{1}^{15}{}_j \, N_j \, \hat{e}_m(\phi_j) \, \hat{e}_n(\phi_j) = \delta_{mn} \tag{7}$$

$$\langle \hat{\underline{e}}_m \underline{e}^*_n \rangle = \frac{1}{N} \sum_{1}^{15}{}_j \, \hat{e}_m(\phi_j) \sum_{1}^{N_j}{}_i \, e^*_n(\lambda_i, \phi_j) = 0 \tag{8}$$

$$\hat{C}_{mp} = \langle \hat{\underline{e}}_m \hat{\underline{z}}_p \rangle = \frac{1}{N} \sum_{1}^{15}{}_j \, N_j \, \hat{e}_m(\phi_j) \, \hat{z}_p(\phi_j) \tag{9}$$

$$\frac{1}{1152} \sum_{1}^{1152}{}_p \, \hat{C}_{mp} \, \hat{C}_{np} = \delta_{mn} \, \hat{V}_m \tag{10}$$

So, even though orthogonality in time is guaranteed only within the two separate sets of zonal and eddy coefficients, zonal and eddy EOFs together form a set of spatial functions that are orthogonal with respect to the same definition of inner product. One must note that only 14 zonal EOFs and 562 eddy EOFs eventually exist, since due to definitions (1b) and (1d) only 14 and 562 independent values are needed to determine a zonal field $\hat{\underline{z}}_p$ or an eddy field $\underline{z}^*_p$, respectively. In addition, all these EOFs are orthogonal to the normalized constant function:

$$e_o(\lambda_i, \phi_j) = 1 \qquad \text{for each } i,j \tag{11}$$

So we can write

$$\underline{z}_p = C_o \underline{e}_o + \sum_{1}^{14}{}_m \hat{C}_{mp} \hat{\underline{e}}_m + \sum_{1}^{562}{}_n C^*_{np} \underline{e}^*_n \qquad (12)$$

$$C_o = z_o = \langle \underline{e}_o \underline{z}_p \rangle \qquad (13a)$$

$$\hat{C}_{mp} = \langle \hat{\underline{e}}_m \underline{z}_p \rangle = \langle \hat{\underline{e}}_m \hat{\underline{z}}_p \rangle \qquad (13b)$$

$$C^*_{mp} = \langle \underline{e}^*_m \underline{z}_p \rangle = \langle \underline{e}^*_m \underline{z}^*_p \rangle \qquad (13c)$$

Both the zonal and the eddy EOFs are ordered, as usual, according to the decreasing amplitude of the associated eigenvalues.

The eddy EOFs 1 to 6 and the zonal EOFs 1 to 3 are presented and discussed in Sections 4 and 5 respectively. In addition, Appendix 2 contains the maps of the first 17 eddy EOFs, whose coefficients have an RMS value exceeding 10 metres, and of the first 5 zonal EOFs, whose coefficients have an RMS value exceeding 5 metres.

3. EVALUATION OF THE SEASONAL CYCLE AND THE INTERANNUAL VARIABILITY OF THE EOF COEFFICIENTS

Since our analysis covers a six-month period of the year, and no time mean field is subtracted from the input values, we may expect to find a relevant variation in both the mean and the rms value of the EOF coefficients from October to March.

Let us write the coefficient of the m-th EOF (either eddy or zonal) as C_{mpq}, where p(=1,...,36) now denotes the pentad number within a given year, and q(=1,...,32) is the index of the year (q=1 represents the period October 1952 through March 1953, and so on). In order to have a smoothed estimate of the seasonal cycle, we computed a "climatological" value of the EOF coefficients for each pentad as:

$$\tilde{C}_{mp} = \frac{1}{96} \sum_{1}^{32} q \; (C_{mp'q} + C_{mpq} + C_{mp''q}) \tag{14}$$

where

$$p' = \max (1, p-1) \tag{15a}$$

$$p'' = \min (36, p+1) \tag{15b}$$

An rms value of the coefficients for each pentad was also computed in an analogous way.

We can then define the "anomaly" of an EOF coefficient as its deviation from $\tilde{C}_{mp}$.

$$C'_{mpq} = C_{mpq} - \tilde{C}_{mp} \tag{16}$$

If, for sake of simplicity, we use the term "variance" as synonymous with "mean square value," we can say that the variance of each coefficient is the sum of the variance accounted for by the seasonal cycle and the variance of the anomaly:

$$V_m = \tilde{V}_m + V'_m \tag{17a}$$

where

$$V_m = \frac{1}{1152} \sum_{1}^{32}{}_q \sum^{36}{}_p (C_{mpq})^2 \qquad (17b)$$

$$\tilde{V}_m = \frac{1}{32} \sum_{1}^{32}{}_p (\tilde{C}_{mp})^2 \qquad (17c)$$

$$V'_m = \frac{1}{1152} \sum_{1}^{32}{}_q \sum^{36}{}_p (C'_{mpq})^2 \qquad (17d)$$

In order to evaluate the relative contributions of the inter-annual and the intra-annual variability to the variance of the anomalies, we also computed bimonthly means of the anomalies for each year in October-November, December-January, and February-March;

$$C''_{m1q} = \frac{1}{12} \sum_{1}^{12}{}_p C'_{mpq} \qquad (18a)$$

$$C''_{m2q} = \frac{1}{12} \sum_{13}^{24}{}_p C'_{mpq} \qquad (18b)$$

$$C''_{m3q} = \frac{1}{12} \sum_{25}^{36}{}_p C'_{mpq} \qquad (18c)$$

and the standard deviations of the 12 pentad values about these means. So the contribution of the interannual variability of long-term means during October-November, for example, can be estimated from the ratio:

$$\left(\frac{V''}{V'}\right)_{m1} = 12 \sum_{1}^{32}{}_q (C''_{m1q})^2 \Big/ \sum_{1}^{32}{}_q \sum_{1}^{12}{}_p (C'_{mpq})^2 \qquad (19)$$

The ratios V_m/V_t (where V_t is the total variance of the eddy or zonal field), $\tilde{V}_m/V_m$, V'_m/V_m, V''_m/V'_m for October-November, December-January, and February-March, respectively, are listed in Table 1 for the first 17 EOF coefficients of the eddies and the first 5 coefficients of the zonal part. The table also shows the rms values of the coefficients and of their anomalies, and the autocorrelation of each coefficient computed with a lag of 1,2, and 3 pentads. The results listed in Table 1 will be discussed in the following sections.

Table 1

No.	V/V_t %	RMS	$\tilde{V}/V$%	V'/V%	RMS'	V''/V'% oc-no	de-ja	fe-ma	r_1	r_2	r_3
a) E.O.F. eddies (total RMS value = 102.0 m)											
1	35.7	61.0	91.5	8.5	17.8	24.7	26.4	23.9	.52	.18	.08
2	7.3	27.5	6.3	93.7	26.6	16.7	27.2	29.9	.61	.26	.13
3	6.3	25.7	11.3	88.7	24.2	23.1	21.1	26.0	.51	.15	.09
4	6.1	25.2	6.0	94.0	24.4	28.3	34.7	22.7	.61	.23	.16
5	4.9	22.5	3.9	96.1	22.1	18.7	22.7	22.1	.62	.26	.12
6	4.2	21.0	1.4	98.6	20.9	24.7	22.9	17.4	.52	.12	.06
7	3.5	19.1	2.2	97.8	18.9	16.6	19.6	23.2	.50	.15	.05
8	3.2	18.4	3.2	96.8	18.1	13.7	20.9	17.0	.41	.09	.06
9	2.8	17.1	5.2	94.8	16.7	25.8	20.3	18.8	.48	.12	.03
10	2.4	15.7	2.4	97.6	15.5	18.1	12.5	23.1	.44	.14	.04
11	1.9	14.1	7.0	93.0	13.6	15.5	13.6	8.9	.31	-.02	-.01
12	1.8	13.8	3.4	96.6	13.6	11.1	10.6	13.5	.22	.01	.02
13	1.6	12.9	5.0	95.0	12.5	15.2	6.6	20.1	.25	-.03	.05
14	1.5	12.3	2.1	97.9	12.2	12.5	14.4	13.4	.27	.06	.04
15	1.4	12.3	9.6	90.4	11.7	13.6	19.2	17.4	.28	.02	.07
16	1.3	11.4	1.2	98.8	11.4	20.0	10.9	16.9	.33	.08	.03
17	1.0	10.0	2.4	97.6	9.9	16.8	12.8	11.7	.23	.09	.06
b) E.O.F. zonal means (total RMS value = 243.5 m)											
1	98.22	241.4	99.5	0.5	17.3	18.6	28.5	28.7	.65	.35	.21
2	1.08	25.4	50.5	49.5	17.8	29.4	31.9	31.1	.61	.33	.25
3	0.47	16.8	9.4	90.6	16.0	18.4	20.4	21.1	.52	.19	.08
4	0.15	9.5	10.0	90.0	9.1	25.1	19.8	24.1	.44	.19	.09
5	0.04	5.1	7.9	92.1	4.9	19.5	15.5	12.4	.31	.17	.13

V = variance of the E.O.F. coefficient

V_t = total variance of the eddy/zonal field

$\tilde{V}$ = variance explained by the seasonal cycle

V' = variance explained by the anomaly

V" = variance explained by the interannual variations of 2-month means

RMS = r.m.s. value of the E.O.F. coefficient (m)

RMS' = r.m.s. value of the anomaly (m)

r_1 = autocorrelation of the anomaly at 1-pentad lag

r_2 = autocorrelation of the anomaly at 2-pentad lag

r_3 = autocorrelation of the anomaly at 3-pentad lag

4. THE EOFs OF THE EDDIES

The first six EOFs of the eddies are shown in Fig. 1, while Fig. 2 shows the mean and the r.m.s. climatological values of the associated coefficients for each pentad of our six-month cold season.

The first EOF is clearly representative of the pattern of 500-mb stationary eddies in winter. The associated time coefficient remains positive in the whole sample of 1152 pentads; as can be seen from Fig. 2 and Table 1a, it explains over 35% of the total eddy variance, but its variability is dominated by the seasonal cycle. Only 8.5% of its variance is explained by the anomaly, whose amplitude is lower than that of the anomalies of other 7 EOF coefficients.

The relative importance of the seasonal cycle and the anomaly is reversed in all the other EOF coefficients of the eddy field. Apart from the slightly lower percentage of the third coefficient, the anomaly explains more than 90 percent of the variance in all of them. We may conclude that the EOFs from number 2 onwards describe transient eddies.

The pattern of EOF 2 is reminiscent of the Pacific North American (PNA) teleconnection pattern as defined by WG. In our analysis, as well as in other observational studies (see Blackmon, et al., 1984), the PNA pattern emerges as the most important component of nonseasonal variability in the winter amtosphere of the northern extratropics. Regarding its seasonal cycle, weak but still statistically significant, we notice that positive values of the coefficient tend to occur more frequently from January to March, negative values from October to December.

EOF 3 is dominated by a zonal wavenumber 1 with maxima at about 60°N over Finland and Alaska. Apart from EOF 1, it has the strongest seasonal cycle in the associated coefficient: the climatological value reaches 15 m in October and -15 m in December, explaining about 10 percent of the variance.

The relevant feature described by EOF 4 is the variable intensity of the Atlantic jet stream. Positive coefficients, which correspond to an increased jet, are more frequent in January and February. In the Atlantic area, this EOF resembles the Western Atlantic (WA) teleconnection pattern as described in WG.

a)

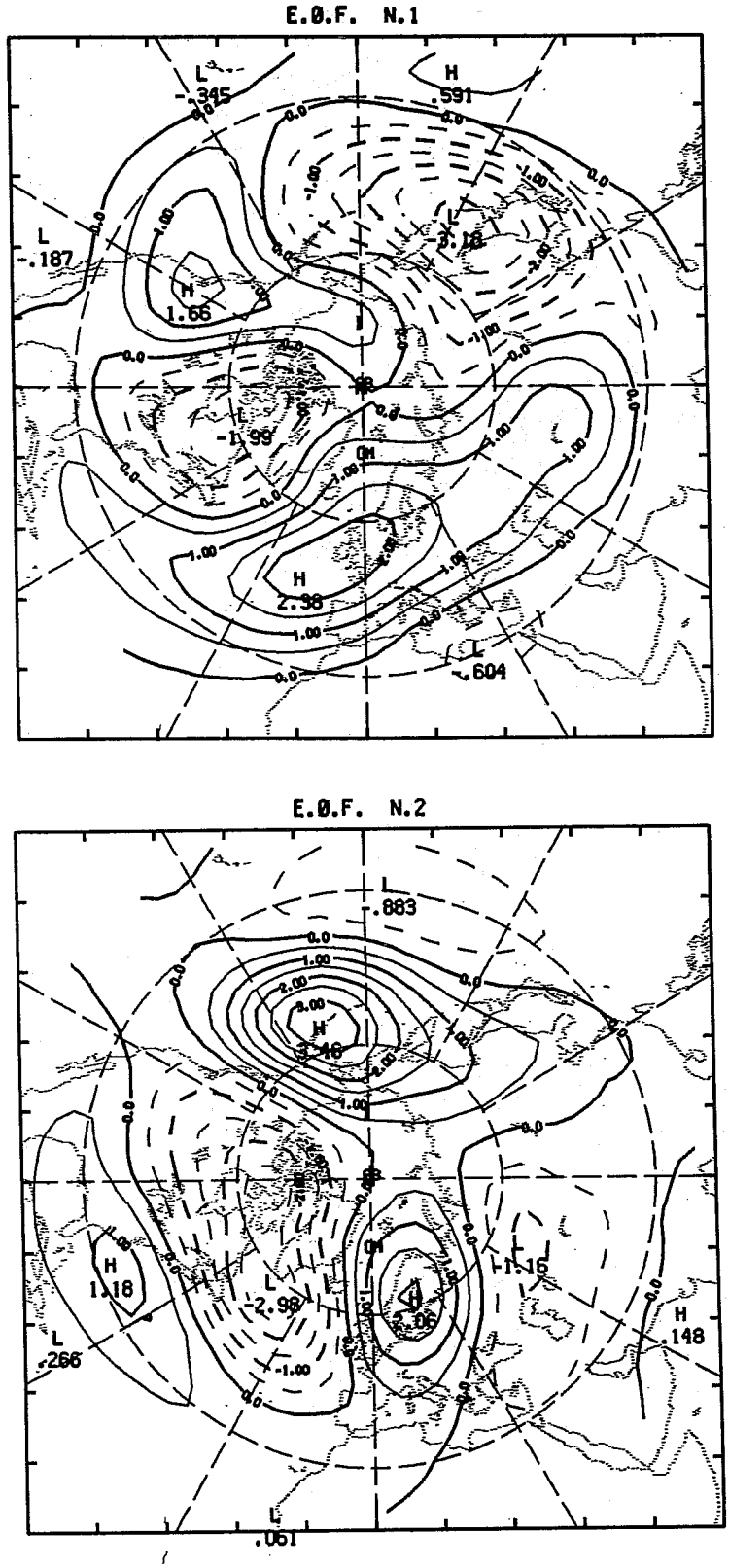

Fig. 1 a) Pattern of eddy EOFs 1 and 2;
b) Pattern of eddy EOFs 3 and 4;
c) Pattern of eddy EOFs 5 and 6.

b)

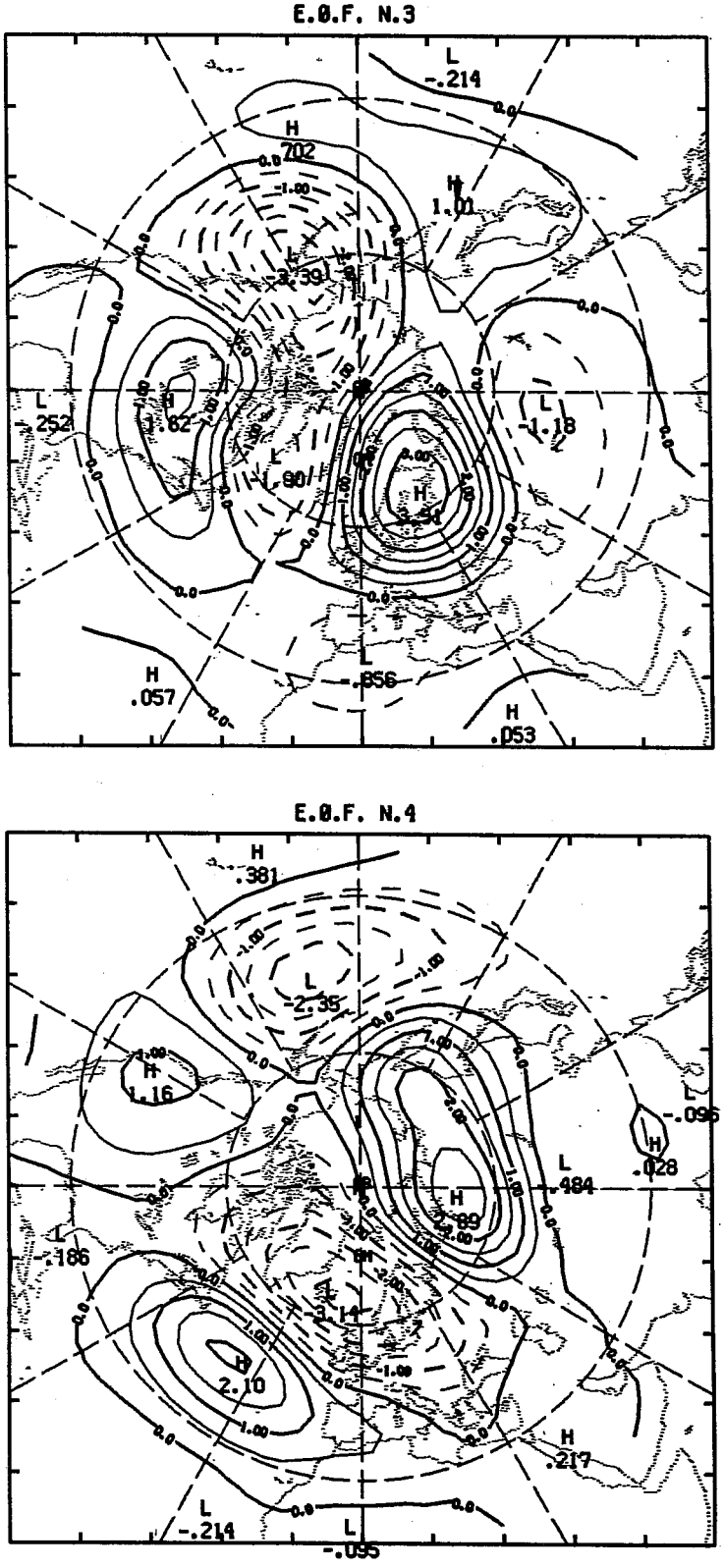

Fig. 1 Continued

C)

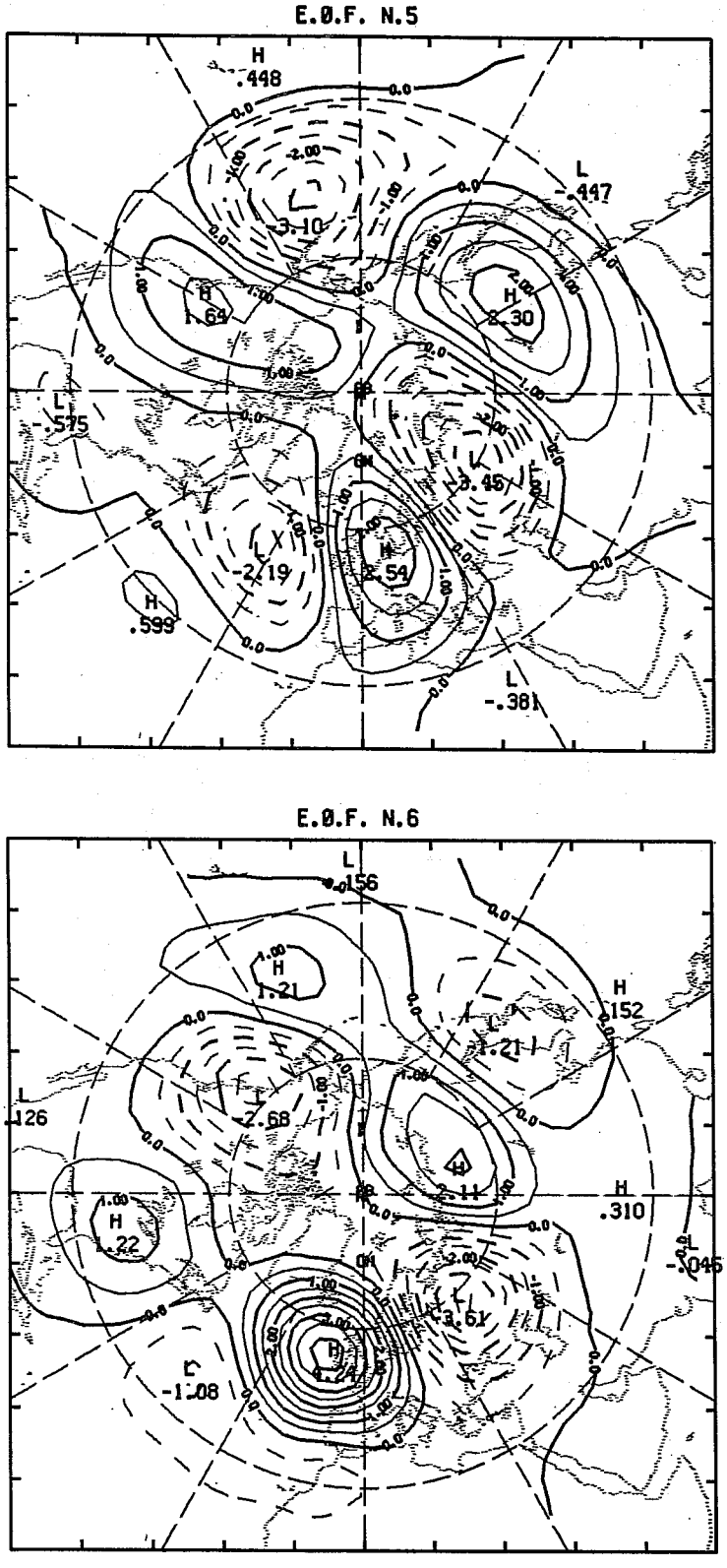

Fig. 1 Continued

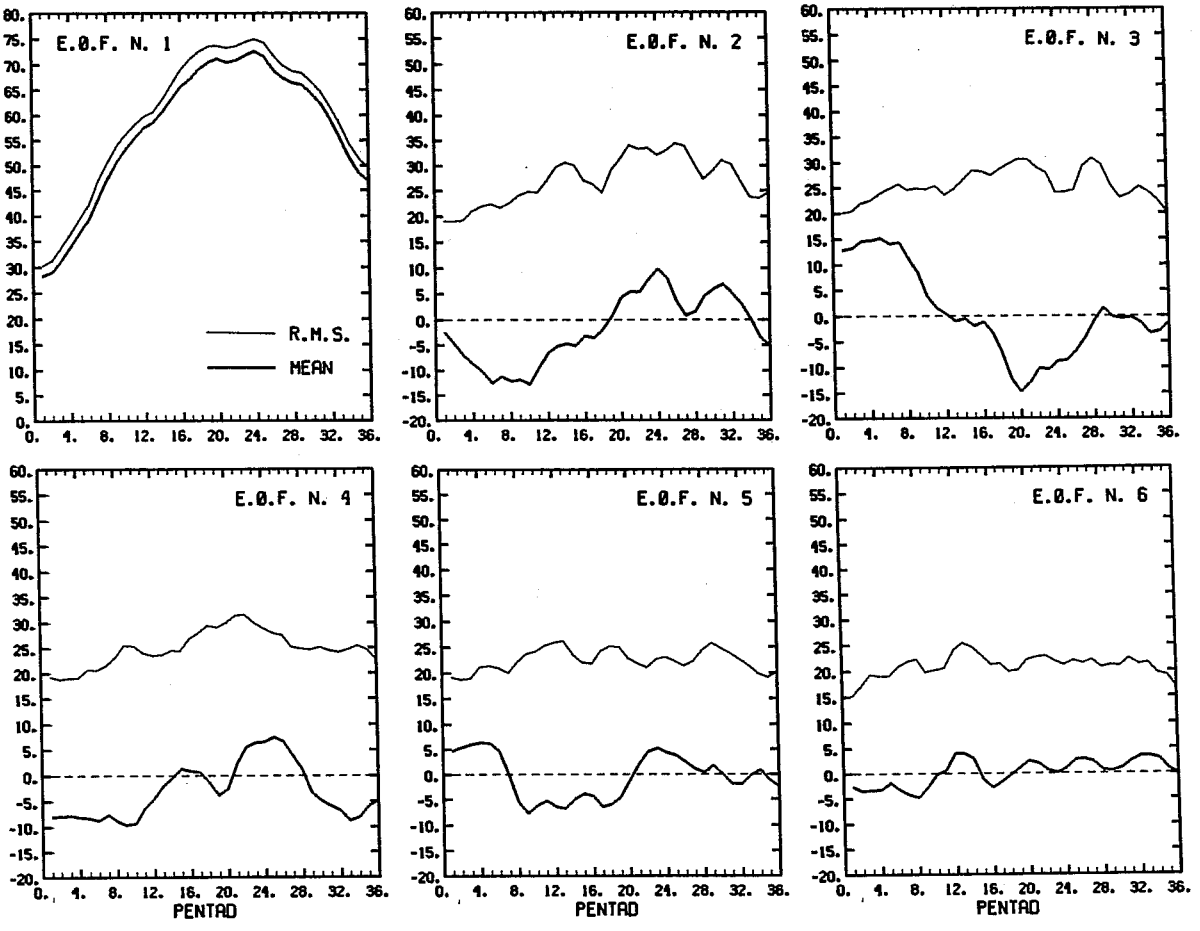

Fig. 2 Mean and r.m.s. climatological values of the coefficients of eddy EOFs 1 through 6 during the cold season from October to March.

The fifth EOF pattern shows a very regular zonal wavenumber 3 with almost no meridional dispersion. The wave maxima are located between 50°N and 60°N; it is interesting to note that simple theories of meridional dispersion of Rossby waves predict the latitudinal confinement of zonal wavenumber 3 if the source of the wave is within this latitude zone (Held, 1983). The amplitude of the seasonal cycle of EOF 5 coefficient is below the level of statistical significance.

From EOF 6 onwards, the EOF patterns tend to include zonal wavenumbers greater than 3, with substantial meridional dispersion and, in many cases, strong localized peaks. These features can be seen in EOF 6, which is worthwhile discussing because its strongest peak is located on the eastern border of the Atlantic Ocean; i.e., a favourable area for the developments of blocking centers. In the Atlantic and Eurasian sector, EOF 6 shows a similar pattern to the Eastern Atlantic (EA) teleconnection (see WG). The seasonal cycle in EOF 6 coefficient is insignificant.

The anomaly autocorrelation coefficients shown in Table 1a indicate EOFs 2, 4 and 5 as the most persistent patterns, with a very similar autocorrelation decay (anomalies of EOFs 1 and 3 are about 10 percent less persistent after 5 and 10 days, and their autocorrelation trend is more similar to that of EOFs 6 and 7).

Regarding the interannual variability of long-term (2-month) means, it generally explains from 20 to 30 percent of the anomaly variance of the dominant EOF coefficients. EOF 4 has the coefficient with the highest percentage of interannual variance in October-November and in December-January, while EOF 2 has the maximum value in February-March.

Figure 3 shows the means and the standard derivation of the anomalies in October-November and in December-January for each of the 32 cold seasons included in our sample. Very high mean values were reached by the EOF 2 coefficient in the winters 1956-57 and 1971-72, probably corresponding to the onset of two major El-Nino episodes as documented by Rasmusson and Carpenter (1982). However, no other peaks are encountered corresponding to two other strong El-Nino events, occurring in 1963-64 and 1982-83 (the 4th coefficient had a strong positive mean value in the latter case). Moreover, according to Horel and Wallace (1982), teleconnections with the northern extratropics are

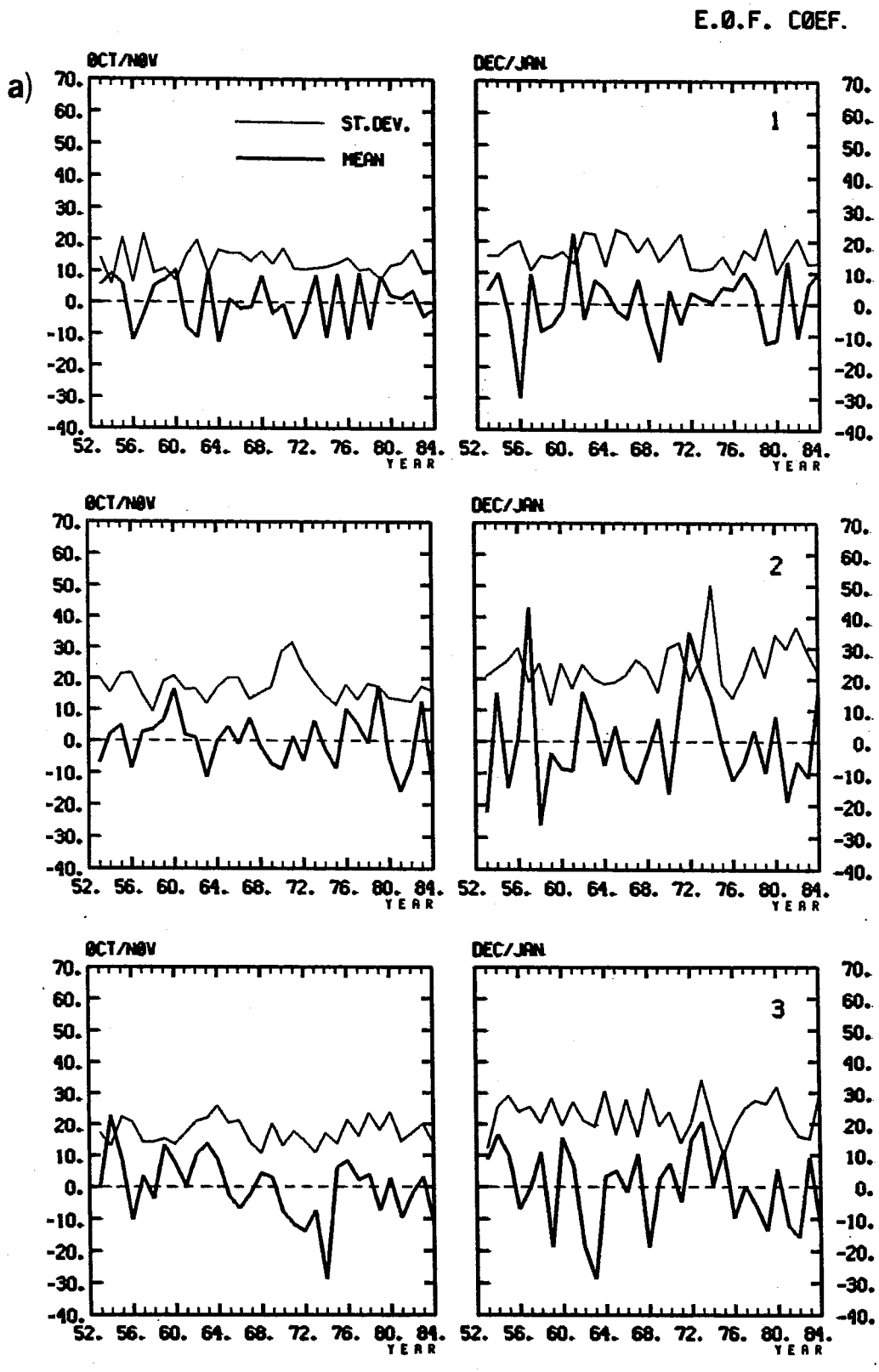

Fig. 3 Means and standard deviations of eddy EOF coefficients 1, 2, and 3(a) and 4, 5 and 6(b), in October-November (left) and December-January (right), for each of the 32 cold seasons in the data sample (from 1952-53 to 1983-94).

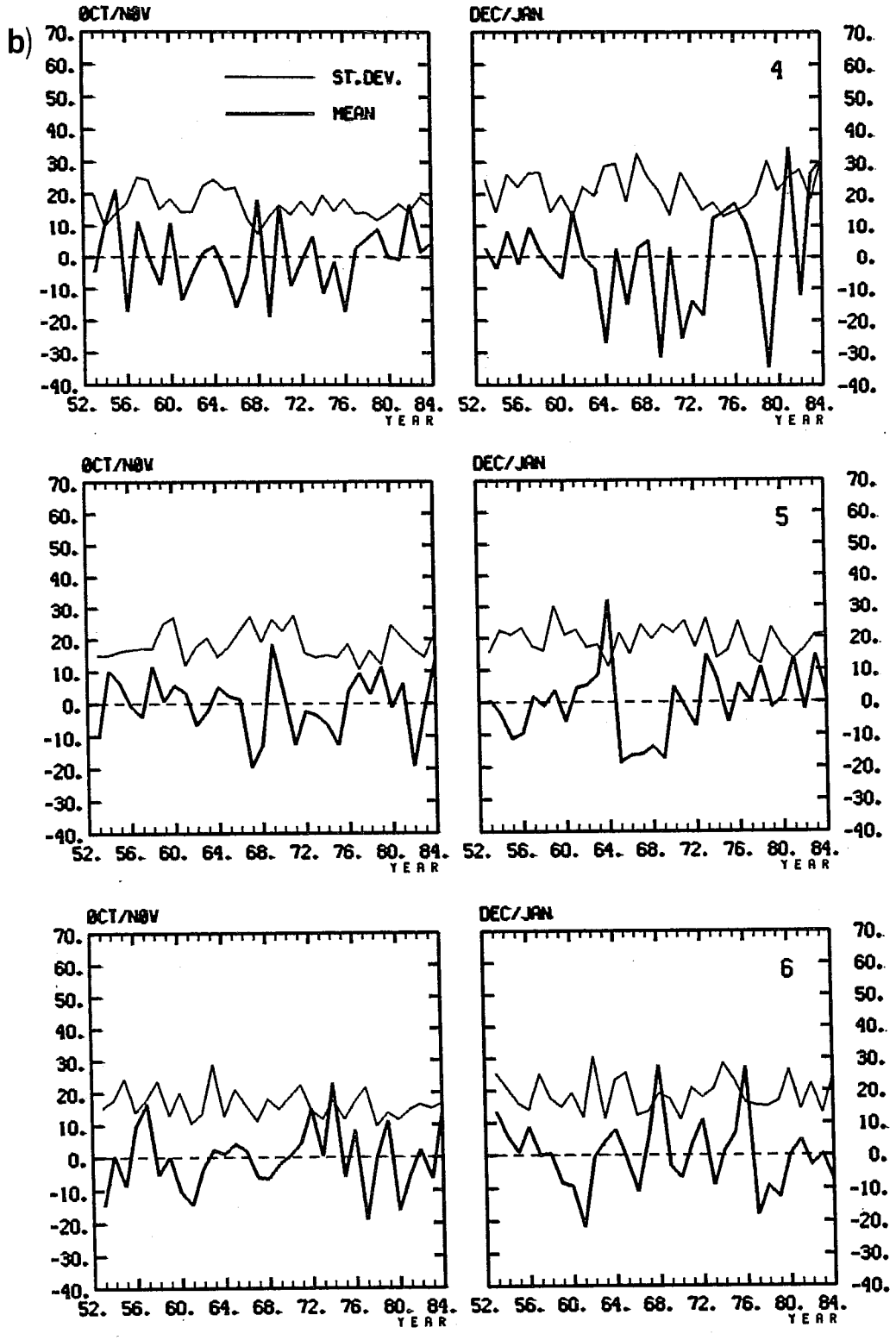

Fig. 3 Continued

more likely to occur in the winter of the subsequent year, when SST and rainfall have reached their maximum in the equatorial central Pacific. Alternative explanations, in addition to tropical thermal forcing, can account for the high interannual variability of EOF 2 and 4. Simmons, et al. (1983) computed normal modes of barotropic equations linearized about the climatological mean 300 mb streamfunction for January. We found relevant similarities between the first and the second mode obtained in their study (see their Fig. 14a, b) and our EOFs 2 and 4, respectively. The first barotropic mode has an e-folding time of 7.3-day, and a period of 40 days, while the second has a 9.8-day e-folding time but an infinite period. In other words, it exhibits a pure exponential growth with no change of phase. These characteristics have a counterpart in the variance distribution of EOF 2 and 4 in December-January. The former explains a higher proportion of the total variance, but the latter is more persistent on long time scales, as shown by the percentage of variance explained by two-month means.

Simmons, et al. (1983) showed that patterns similar to these two modes can also be obtained as the nonlinear response to a diabatic forcing in the equatorial Pacific. Therefore, barotropic instability and thermal forcing can be seen as a complementary, rather than mutually exclusive, explanation for the high inter-annual variability of EOFs 2 and 4.

Finally we can compare our EOFs with those obtained in previous similar studies. In the EOF analysis performed by Rinne and Karhila, (1979; see also Rinne et al., 1981), 11876 analyses of instantaneous 500-mb height fields were used, covering a 20-year period up to 1970 with all the seasons included. The area covered is the same as that used in our study. Since the authors subtracted a single climatological mean field for the whole year from their data, at least the first 2 EOFs are needed to account for the seasonal variations. Apart from those and from our first EOF, relevant similarities can be found between the other EOFs, in particular between their 3rd and our 2nd, their 4th and our 4th, their 8th and our 6th. With regard to this last pattern, their study also confirms the presence of a strong localized source of variance in the eastern Atlantic.

The correspondence between our 2nd and 4th EOF and the dominant barotropically unstable modes finds a strong confirmation in the statistical-dynamical approach of Schubert (1983). Despite the fact that he used streamfunction

(rather than height) fields at 500 mb for his EOF analysis, a good correspondence can be seen between his 2nd, 3rd, 5th and our 2nd, 4th and 3rd EOF, respectively. There is also a strong similarity between his 9th and our 6th EOF over the Atlantic. Schubert's analysis confirms that the first two EOFs are the most barotropically unstable, and the value that he obtained for the e-folding time of his 3rd (our 4th) EOF using a 1-10 January mean field as a basic state is nearly identical (9.9 days against 9.8) to that computed by Simmons, et al. (1983) for their very similar second mode. However, positive growth rates were found up to the 13th EOF.

Therefore, we can conclude that, apart from some differences due to sample fluctuations and analysis procedures, the patterns represented in our EOFs of 500 mb height eddies are common to a number of other observational studies concerning the low frequency variability of the atmosphere. Their relevance is confirmed by the resemblance of some of them to the most barotropically unstable linear modes of the northern extratropical atmosphere in winter. In addition, estimates of the probability density functions of the eddy EOF coefficients, discussed in Molteni et al. (1987), have revealed bimodal distributions that provide observational support to the theories on the existence of multiple equilibria states in the wintertime extratropical circulation (e.g. Charney and De Vore, 1979, Benzi et al., 1986).

5. THE EOFs OF THE ZONAL MEANS

The first 3 EOFs of the zonal means of 500 mb height and the seasonal variations in the mean and r.m.s. values of their coefficients are shown in Fig. 4 and Fig. 5 respectively. The variance data reported in table 1b reveal that these 3 EOF are nearly equally important in describing the anomalous variations of the zonal mean profile, while the mean seasonal variations produce a strong dominance of the first EOF in the total variance.

In fact, the first EOF represents the latitudinal gradient of the height field between the tropics and the pole, and its coefficient is an index of the intensity of the latitudinally-averaged westerly flow. It reaches the climatological maximum in December, after a steep increase in October and November.

The pattern of zonal EOF 2 shows a positive gradient of height south of 45°N and a negative gradient north of that latitude. So, positive coefficients of this EOF are associated with a northern position of the jet, negative values with a southern location; the most southern position is reached at the end of January. The seasonal cycle and the anomaly account for almost equal proportions of the variance of the coefficient.

The structure of zonal EOF 3 is representative of a tendency towards a split of the jet in two parts, with decreased westerlies between 40° and 60°N, when the associated coefficient is positive; negative coefficients correspond to the concentration of the jet around 50°N and to polar easterlies when a sufficient amplitude (about 20 m in Jan and Feb) is reached. One might expect to find an association between large positive values of EOF 3 coefficient and globally-blocked circulation patterns. The sign of the coefficient is, on average, negative before the winter solstice, positive afterwards, but the seasonal cycle accounts for only 10% of its variance.

The interannual variations of bimonthly means and standard deviations of the anomalies are shown in Fig. 6. This figure and the data of Table 1b show that, among the zonal EOFs, the second one has the greatest proportion of interannual variability in the whole cold season. The difference is more relevant in Oct.-Nov., while in the other months the interannual variance of the first EOF is only 10% lower. The proportions of variance explained by the interannual variations for these two zonal EOFs are comparable (~ 30%) to

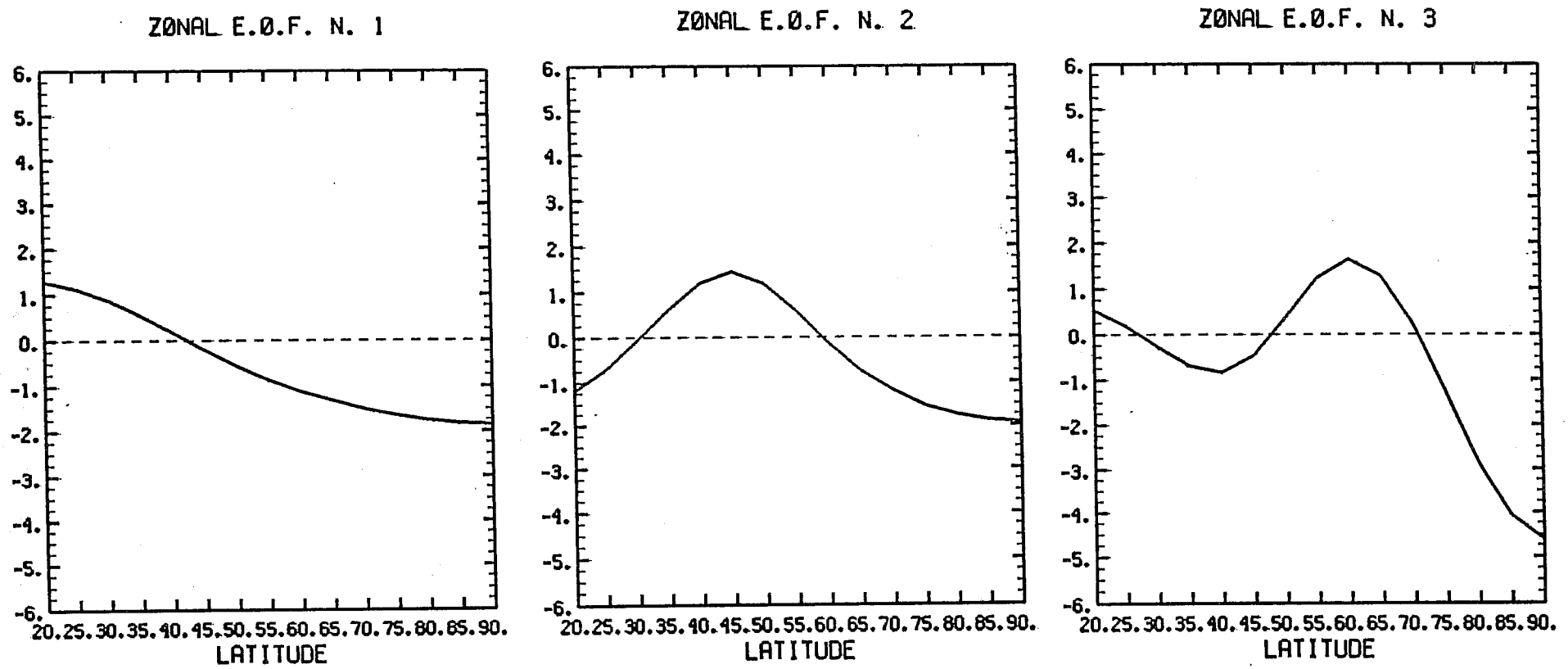

Fig. 4 Pattern of the first three zonal EOFs.

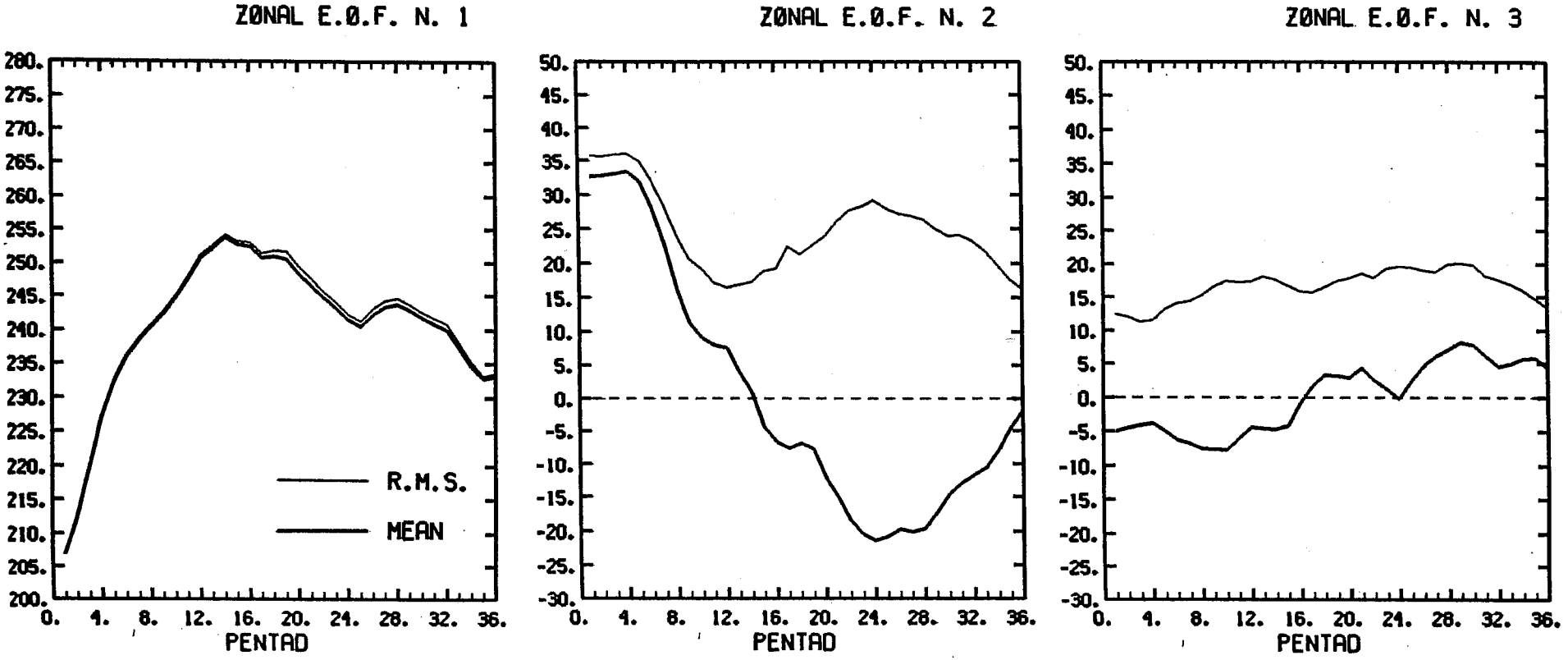

Fig. 5 Mean and r.m.s. climatological values of the coefficient of zonal EOFs 1, 2 and 3 during the cold season from October to March.

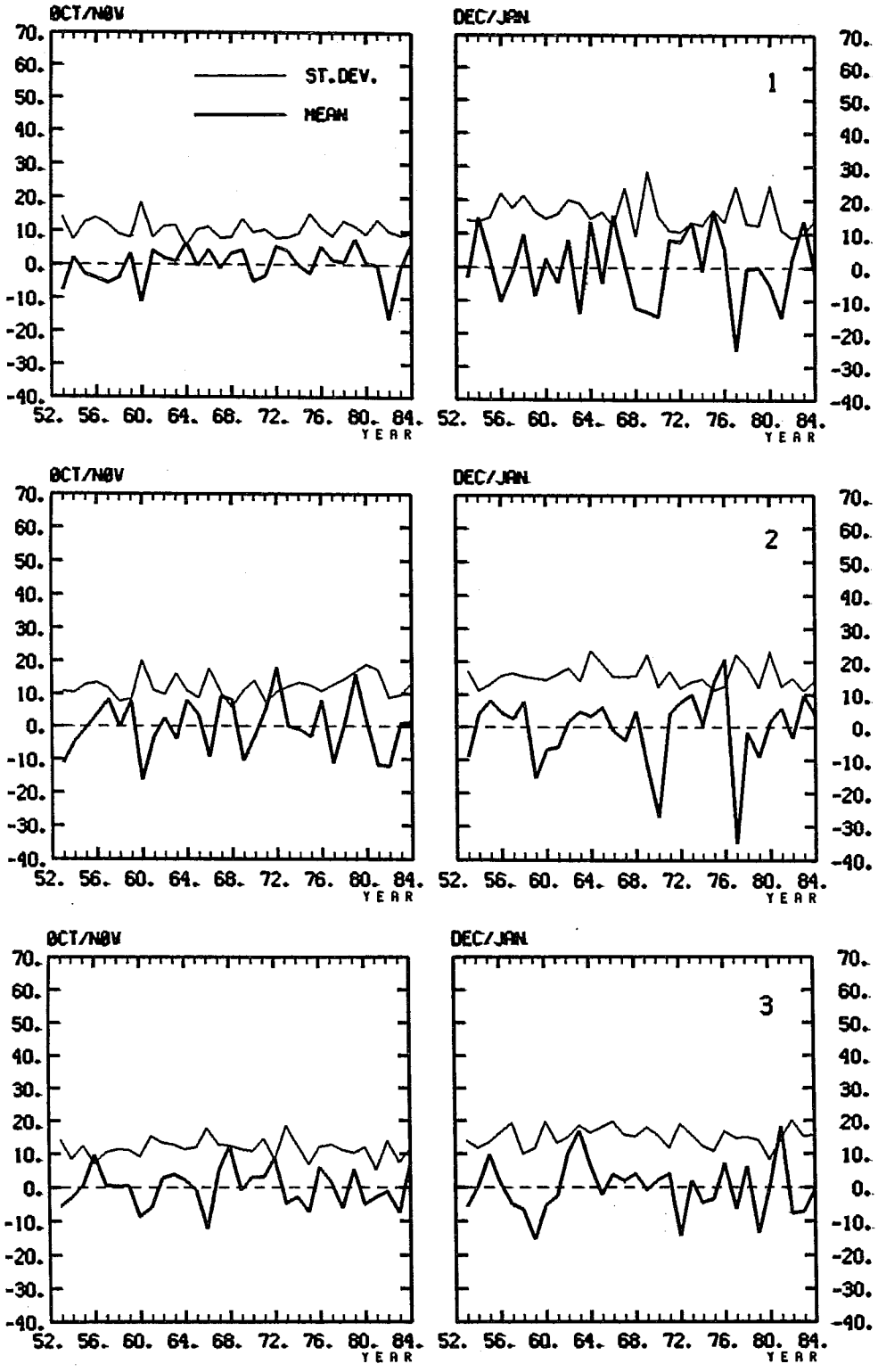

Fig. 6 Means and standard deviations of zonal EOF coefficients 1, 2 and 3 in October-November (left) and December-January (right), for each of the 32 cold seasons in the data sample (from 1952-53 to 1983-84).

those found for the 2nd and the 4th EOFs of the eddies, even if the values of the zonal EOF 2 show a distinctive and remarkable stability during the six-month period.

The coefficients of the first two zonal EOFs have a similar behaviour also with regard to the medium-term persistence of the anomaly, as shown by the autocorrelation indices of table 1b. They are clearly more persistent than the 2nd, 4th or 5th eddy coefficients after 2 or 3 pentads.

6. SUMMARY AND CONCLUSIONS

In this work, the fields of geopotential height in the northern extratropics were decomposed into a spatially constant, a zonally averaged and an eddy component, and EOF analyses were performed separately on the zonal and the eddy fields. This procedure allowed the evaluation of modes of variability of the atmospheric circulation (principally, the variations in the intensity of the mean zonal flow, in its latitudinal structure and in the amplitude of the stationary waves) that cannot be easily studied using the traditional, anomaly-based EOF approach.

An analysis of the variance distribution of the EOF coefficients showed that the eddy patterns account for the greatest proportions of the low-frequency variance in the northern hemisphere. There are significant similarities between a number of eddy EOFs and teleconnection patterns identified in previous observational studies. Some of them (namely, the 2nd and the 4th eddy EOF) also resemble the most barotropically unstable linear modes of the wintertime extratropical circulation, and a considerable proportion of their variance is explained by interannual variability. The pattern of the 5th eddy EOF resembles a zonal wavenumber 3 with a latitudinally confined amplitude, and might be explained by resonance phenomena invoked by the theories on multiple equilibria.

Interannual variations are also relevant for the first two zonal EOFs, whose coefficients are indices of the mean intensity of the westerly flow and of the position of its maximum, respectively. These coefficients show the greatest autocorrelation after 10 and 15 days among all the eddy and zonal EOFs, even when the seasonal cycle is subtracted.

The fact that the patterns of a number of EOFs obtained in this work have been revealed in other studies on the low-frequency variability of the atmosphere does not necessarily imply a particular physical meaning for each single EOF. But undoubtedly, the most important EOFs determine, in an efficient way, a subspace of limited dimension on which we can project the large scale atmospheric fields retaining physically relevant modes of variability. This synthetic representation can be a very useful starting point for diagnostic studies or verifications of theories and numerical experiments.

Acknowledgements

This work was planned with A. Sutera when he was a visiting scientist at ECMWF; his collaboration in the evaluation of the results is gratefully acknowledged. N. Tronci provided computational and graphical assistance. The author is also grateful to S. Tibaldi and T.N. Palmer for frequent and constructive discussions, and to C. Brankovic for his help in data retrieval.

References

Benzi, R., P. Malguzzi, A. Speranza, and A. Sutera, 1986: The statistical properties of general atmospheric circulation: Observational evidence and a minimal theory of bimodality. Quart.J.Roy.Meteorol.Soc., 112, 661-676.

Buell, C.E., 1975: The topography of empirical orthogonal functions. Preprints Fourth Conf. Probability and Statistics in Atmospheric Sciences, November 18-21, Tallahassee, Fl., Amer. Meteor. Soc., 188-193.

Buell, C.E., 1979: On the physical interpretation of empirical orthogonal functions. Preprints Sixth Conf. Probability and Statistics in Atmospheric Sciences, Banff, Alta, Canada. Amer. Meteor. Soc., 112-117.

Blackmon, M.L., Y.H. Lee, and J.M. Wallace, 1984: Horizontal structure of 500 mb height fluctuations with long, intermediate and short time scales. J.Atmos.Sci., 46, 961-979.

Charney, J.G. and J.G. DeVore, 1979: Multiple flow equilibria in the atmosphere and blocking. J.Atmos.Sci., 36, 1205-1216.

Held, I.M., 1983: Stationary and quasi-stationary eddies in the extratropical troposphere: Theory. Large Scales Dynamical Processes in the Atmosphere B. Hoskins and R. Pierce, Eds., Academic Press, 127-168.

Horel, J.D. and J.M. Wallace, 1981: Planetary scale atmospheric phenomena associated with southern oscillation. Mon.Wea.Rev., 109, 8130-829.

Molteni, F., A. Sutera and N. Tronci, 1987: EOFs of the geopotential eddies at 500 mb in winter and their probability density distributions. Submitted to the Journal of Atmospheric Sciences.

Rasmusson, E.M. and T.M. Carpenter, 1982: Variations in tropical sea surface temperatures and surface wind fields associated with the southern oscillation/El Nino. Mon.Wea.Rev., 110, 354-384.

Rinne, J. and V. Karhila, 1979: Empirical orthogonal functions of 500 mb height in the northern hemisphere determined from a large data sample. Quart.J.Roy.Meteor.Soc., 105, 873-884.

Rinne, J., V. Karhila and S. Jarvenoja, 1981: The EOFs of the 500 mb height in the extratropics of the northern hemisphere. Report No. 17, Dept. of Meteorology, University of Helsinki, Finland.

Schubert, S.D., 1983: A statistical-dynamical study of the large-scale intraseasonal variability of the northern hemisphere winter circulation. Scientific Report NO 3, Department of Meteorology, University of Wisconsin, Madison, USA, 184 pp.

Simmons, A.J., J.M. Wallace, and G.W. Branstator, 1983: Barotropic wave propagation and instability and atmospheric teleconnection patterns. J.Atmos.Sci., 40, 1363-1392.

Wallace, J.H., P. Ambrozy, C. Brankovic, H. Edmon, R.Jenne, E. Oriol, and P. Price, 1983: Five day mean 500 mb height and sea level pressure fields for the northern hemisphere (1946-1977). Long-range Forecasting Research Publication Series No. 2, World Meteorological Organization, Geneva, 257 pp.

Wallace, J.M., and D.S. Gutzler, 1981: Teleconnection in the geopotential height field during the northern hemisphere winter. Mon.Wea.Rev., 109, 784-812.

APPENDIX 1

Spatially weighted EOF analysis

This appendix describes a simple technique allowing the computation of empirical functions that are spatially orthonormal with respect to a weighted inner product:

$$\langle \underline{f}_1, \underline{f}_2 \rangle = \sum_k w(\underline{x}_k)\, f_1(\underline{x}_k)\, f_2(\underline{x}_k) \qquad \text{(A1)}$$

where:

$$w(\underline{x}_k) \neq 0 \qquad \text{for } k = 1, \ldots, N$$

$$\sum_k w(\underline{x}_k) = 1.$$

If $z_t(\underline{x}_k)$ is the value of the field that one wants to analyse, at time t and on the point $\underline{x}_k$, let us define:

$$z'_t(\underline{x}_k) = z_t(\underline{x}_k) \cdot \sqrt{w(\underline{x}_k)} \qquad \text{(A2)}$$

If one performs a normal EOF analysis on the z' fields, the result is a set of eigenvectors $\underline{e}'_m$ (m = 1, ..., N) and a corresponding set of time coefficients C'_{mt} with the following properties:

$$\sum_k e'_m(\underline{x}_k)\, e'_n(\underline{x}_k) = \delta_{mn} \qquad \text{(A3)}$$

$$C'_{mt} = \sum_k e'_m(\underline{x}_k)\, z'_t(\underline{x}_k) \qquad \text{(A4)}$$

$$\sum_t C'_{mt}\, C'_{nt} = \delta_{mn}\, L_m \qquad \text{(A5)}$$

where L_m is the eigenvalue associated with $\underline{e}_m$.
If is sufficient to define:

$$e_m(\underline{x}_k) = e'_m(\underline{x}_k) \,/\, \sqrt{w(\underline{x}_k)} \qquad \text{(A6)}$$

in order to have the following properties verified:

$$\langle \underline{e}_m, \underline{e}_n \rangle = \sum_k w(\underline{x}_k)\, e_m(\underline{x}_k)\, e_n(\underline{x}_k) =$$

$$= \sum_k e'_m(\underline{x}_k)\, e'_n(\underline{x}_k) = \delta_{mn} \qquad \text{(A7)}$$

$$C_{mt} = \langle \underline{e}_m, \underline{z}_t \rangle = \sum_k w(\underline{x}_k)\, e_m(\underline{x}_k)\, z_t(\underline{x}_k) =$$

$$= \sum_k e'_m(\underline{x}_k)\, z'_t(\underline{x}_k) = C'_{mt} \qquad \text{(A8)}$$

So, both the spatial orthogonality according to (A1) and the time orthogonality (with the usual metrics) are satisfied. The total variance of the time coefficients will be equal to a weighted mean of the variance of $\underline{z}_t$ in the individual points:

$$\sum_m \sum_t C^2_{mt} = \sum_k w(\underline{x}_k) \sum_t z^2_t(\underline{x}_k) \qquad \text{(A9)}$$

APPENDIX 2

Patterns of Eddy EOFs 1-17 and Zonal EOFs 1-5

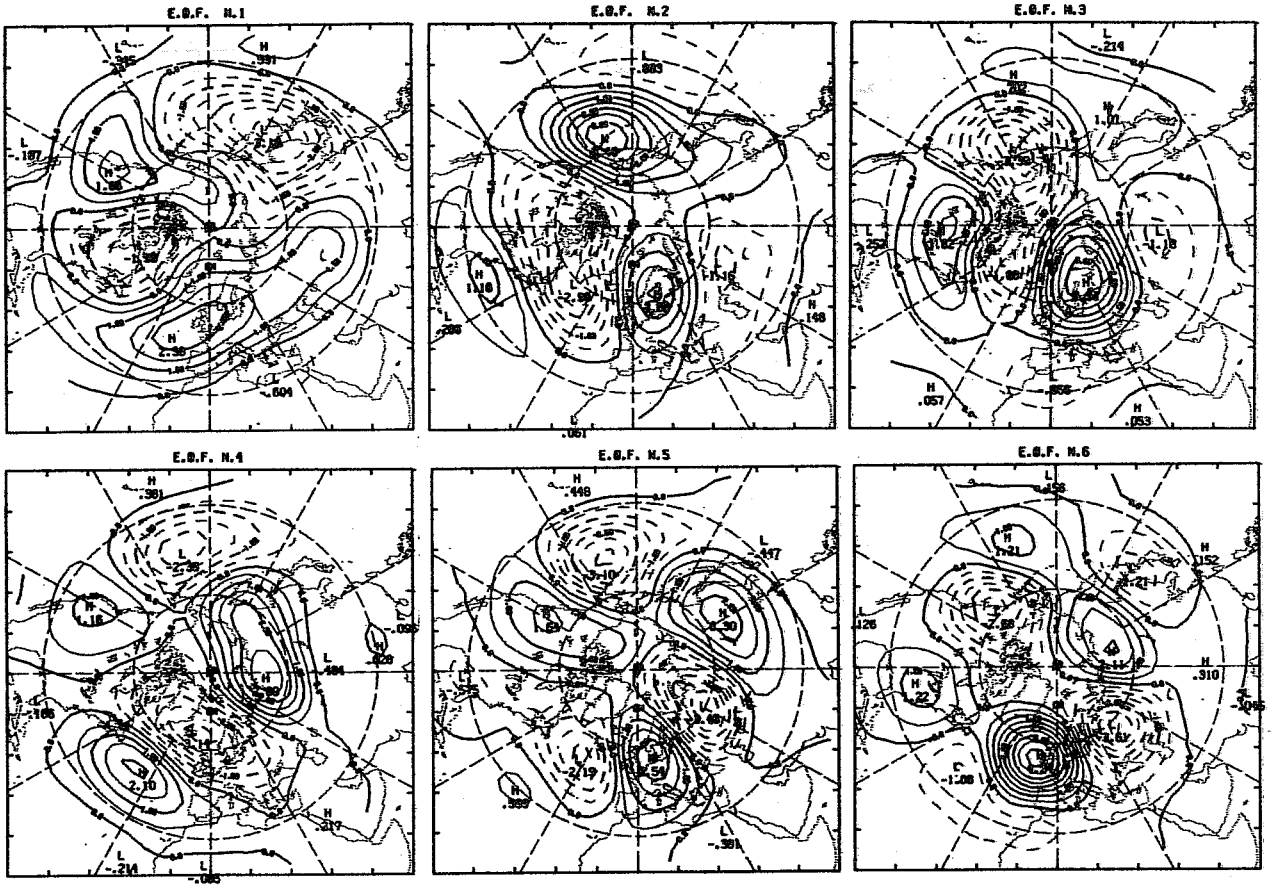

Fig. A1 Patterns of eddy EOFs 1 to 15

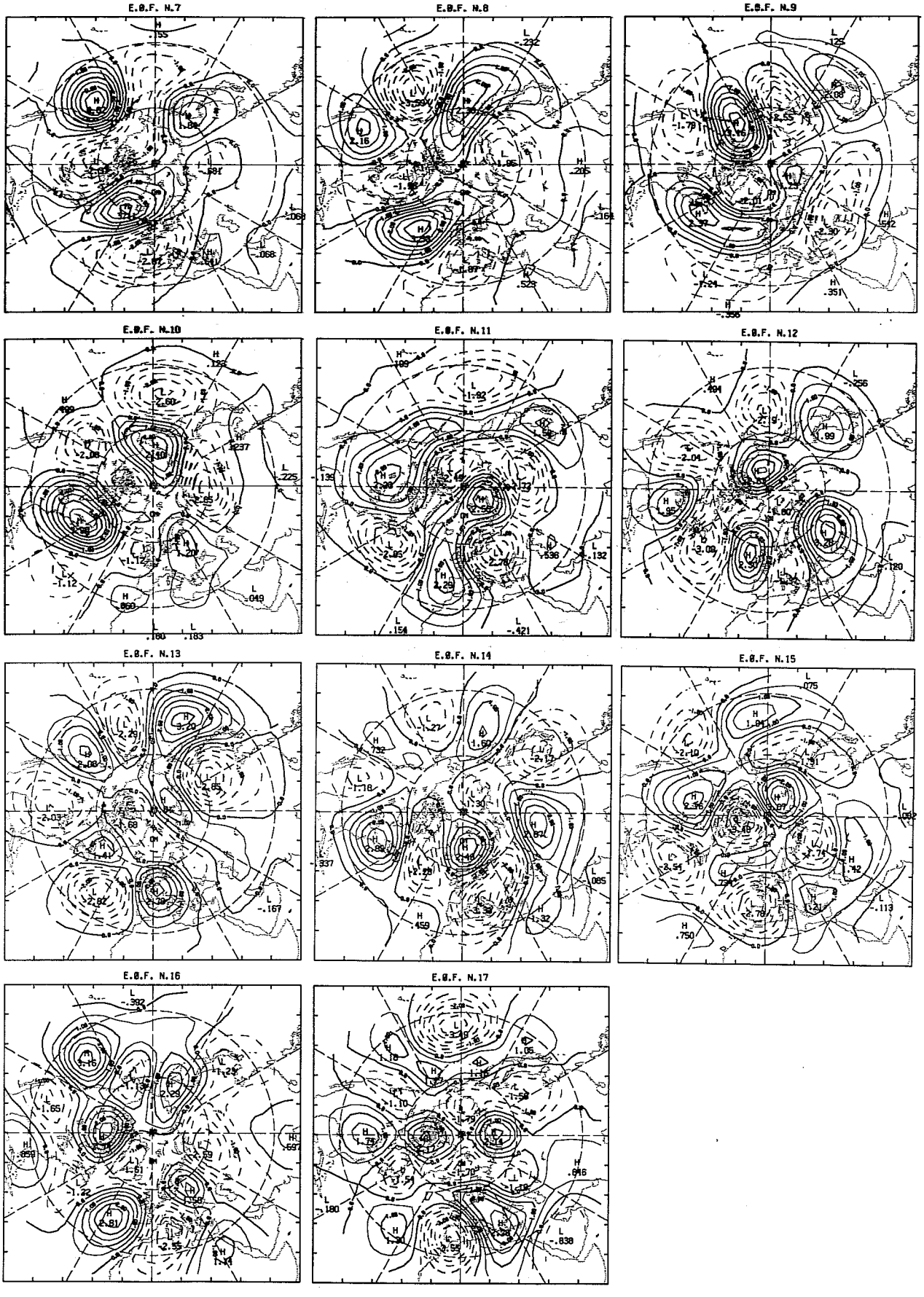

Fig. A1 Continued

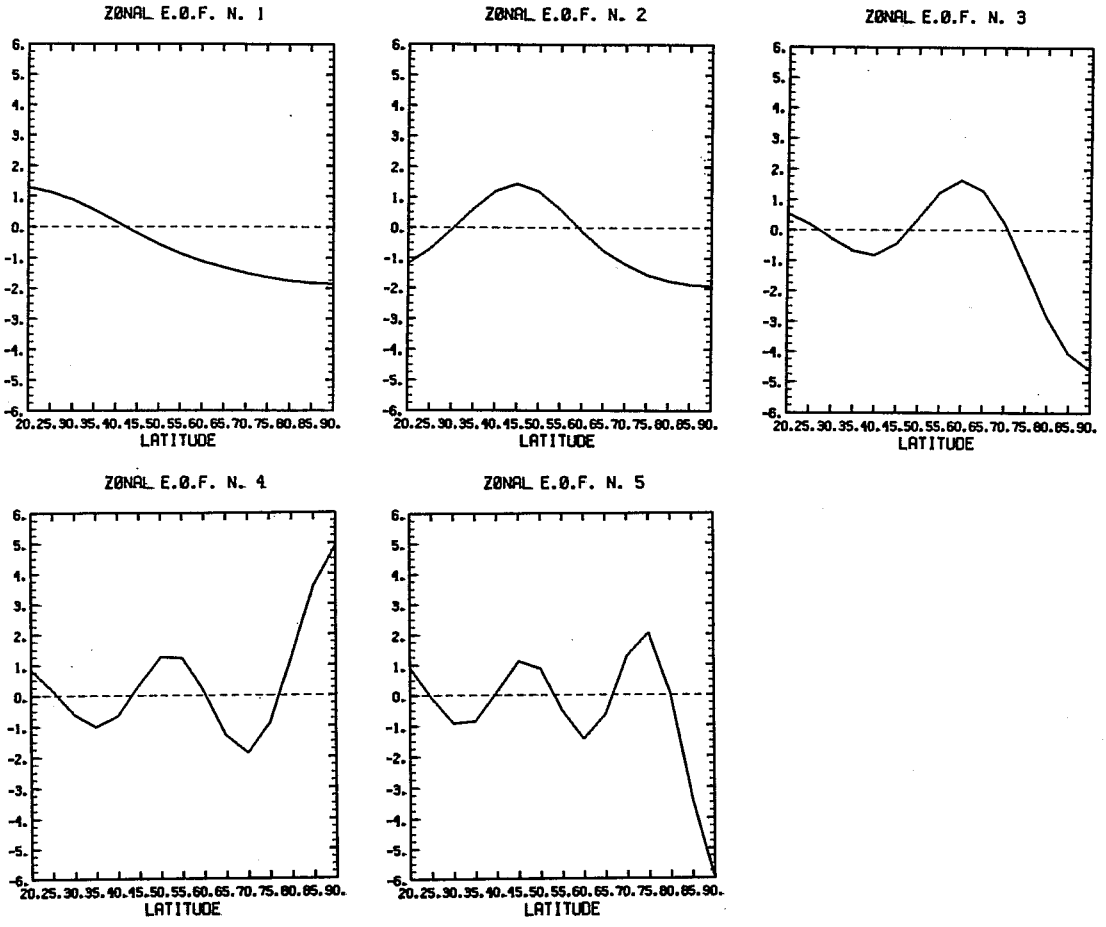

Fig. A2 Patterns of zonal EOFs 1 to 5

ECMWF PUBLISHED TECHNICAL REPORTS

No.1 A case study of a ten day prediction. (Arpe, K., L. Bengtsson, A. Hollingsworth and J. Janjic; September, 1976)

No.2 The effect of arithmetic precisions on some meteorological integrations. (Baede, A.P.M., D. Dent and A. Hollingsworth; December 1976)

No.3 Mixed-radix fast Fourier transforms without reordering. (Temperton, C.; February, 1977)

No.4 A model for medium-range weather forecasting - adiabatic formulation. (Burridge, D.M., and J. Haseler; March 1977)

No.5 A study of some parameterisations of sub-grid processes in a baroclinic wave in a two-dimensional model. (Hollingsworth, A.; July, 1977)

No.6 The ECMWF analysis and data assimilation scheme: analysis of mass and wind field. (Lorenc, A., I. Rutherford and G. Larsen; December, 1977)

No.7 A ten-day high-resolution non-adiabatic spectral integration; a comparative study. (Baede, A.P.M., and A.W. Hansen; October, 1977)

No.8 On the asymptotic behaviour of simple stochastic-dynamic systems. (Wiin-Nielsen, A.; November, 1977

No.9 On balance requirements as initial conditions. (Wiin-Nielsen, A.; October, 1978)

No.10 ECMWF model - parameterization of sub-grid scale processes. (Tiedtke, M., J.-F. Geleynn, A. Hollingsworth and J.-F. Louis; January, 1979)

No.11 Normal mode initialization for a multi-level grid-point model. (Temperton,C., and D. L. Williamson; April, 1979)

No.12 Data assimilation experiments. (Seaman, R.; October, 1978)

No.13 Comparison of medium range forecasts made with two parameterization schemes. (Hollingsworth, A., K. Arpe, M. Tiedtke, M. Capaldo, H. Savijärvi, O. Åkesson, and J.A. Woods; 1978)

No.14 On initial conditions for non-hydrostatic models. (Wiin-Nielsen, A.C.; November, 1978)

No.15 Adiabatic formulation and organization of ECMWF's spectral model. (Baede, A.P.M., M. Jarraud and U. Cubasch; 1979)

No.16 Model studies of a developing boundary layer over the ocean. (Okland, H.; November, 1979)

No.17 The response of a global barotropic model to forcing by large-scale orography. (Quiby, J.; January, 1980)

No.18 Confidence limits for verification and energetics studies. (Arpe, K.; May, 1980)

No.19 A low order barotropic model on the sphere with orographic and Newtonian forcing. (Källén, E.; July, 1980)

No.20 A review of the normal mode initialization method. (Du H, X.Y.; August, 1980)

No.21 The adjoint equation technique applied to meteorological problems. (Kontarev, G.; September, 1980)

No.22 The use of empirical methods for mesoscale pressure forecasts. (Bergthorsson, P.; November, 1980)

No.23 Comparison of medium range forecasts made with models using spectral or finite difference techniques in the horizontal. (Jarraud, M., C. Girard, and U. Cubasch; February, 1981)

No.24 On the average errors of an ensemble of forecasts. (Derome, J.; February, 1981)

No.25 On the atmospheric factors affecting the Levantine Sea. (Ozsoy, E.; May, 1981)

No.26 Tropical influences on stationary wave motion in middle and high latitudes. (Simmons, A.J.; August, 1981)

No.27 The energy budgets in North America, North Atlantic and Europe based on ECMWF analyses and forecasts. (Savijärvi, H.; November, 1981)

No.28 An energy and angular momentum conserving finite-difference scheme, hybrid coordinates and medium-range weather prediction. (Simmons, A.J., and R. Strüfing; November, 1981)

No.29 Orographic influences on Mediterranean lee cyclogenesis and European blocking in a global numerical model. (Tibaldi, S. and A. Buzzi; February, 1982)

No.30 Review and re-assessment of ECNET - A private network with open architecture. (Haag, A., F. Königshofer and P. Quoilin; May, 1982;)

No.31 An investigation of the impact at middle and high latitudes of tropical forecast errors. (Haseler, J.; August, 1982)

No.32 Short and medium range forecast differences between a spectral and grid point model. An extensive quasi-operational comparison. (Girard, C. and M. Jarraud; August, 1982)

No.33 Numerical simulations of a case of blocking: the effects of orography and land-sea contrast. (Ji, L.R., and S. Tibaldi; September, 1982)

No.34 The impact of cloud track wind data on global analyses and medium range forecasts. (Källberg, P., S. Uppala, N. Gustafsson and J. Pailleux; December, 1982)

No.35 Energy budget calculations at ECMWF: Part I: Analyses 1980-81 (Oriol, E.; December, 1982)

No.36 Operational verification of ECMWF forecast fields and results for 1980-1981. (Nieminen, R.; February, 1983)

No.37 High resolution experiments with the ECMWF model: a case study. (Dell'Osso, L.; September, 1983)

No.38 The response of the ECMWF global model to the El-Nino anomaly in extended range prediction experiments. (Cubasch, U.; September, 1983)

No.39 On the parameterisation of vertical diffusion in large-scale atmospheric models. (Manton, M.J.; December, 1983)

No.40 Spectral characteristics of the ECMWF objective analysis system. (Daley, R.; December, 1983)

No.41 Systematic errors in the baroclinic waves of the ECMWF model. (Klinker, E., and M. Capaldo; February, 1984)

No.42 On long stationary and transient atmospheric waves. (Wiin-Nielsen, A.C.; August, 1984)

No.43 A new convective adjustment scheme. (Betts, A.K., and M.J. Miller; October, 1984)

No.44 Numerical experiments on the simulation of the 1979 Asian summer monsoon. (Mohanty, U.C., R.P. Pearce and M. Tiedtke; October, 1984)

No.45 The effect of mechanical forcing on the formation of a mesosale vortex. (Wu, G.X., and S.J. Chen; October, 1984)

No.46 Cloud prediction in the ECMWF model. (Slingo, J., and B. Ritter; January, 1985)

No.47 Impact of aircraft wind data on ECMWF analyses and forecasts during the FGGE period. 8-19 November 1979. (Baede, A.P.M., P. Kållberg, and S. Uppala; March, 1985)

No.48 A numerical case study of East Asian coastal cyclogenesis. (Chen, S.J. and L. Dell'Osso; May, 1985)

No.49 A study of the predictability of the ECMWF operational forecast model in the tropics. (Kanamitsu, M.; September, 1985)

No.50 On the development of orographic cyclones. (Radinovic, D.; June, 1985)

No.51 Climatology and systematic error of rainfall forecasts at ECMWF. (Molteni, F., and S. Tibaldi; October, 1985)

No.52 Impact of modified physical processes on the tropical simulation in the ECMWF model. (Mohanty, U.C., J.M. Slingo and M. Tiedtke; October, 1985)

No.53 The performance and systematic errors of the ECMWF tropical forecasts (1982-1984). (Heckley, W.A.,; November, 1985)

No.54 Finite element schemes for the vertical discretization of the ECMWF forecast model using linear elements. (Burridge, D.M., J. Steppeler, and R. Strüfing; January, 1986)

No.55 Finite element schemes for the vertical discretization of the ECMWF forecast model using quadratic and cubic elements. (Steppeler, J.; February, 1986)

No.56 Sensitivity of medium-range weather forecasts to the use of an envelope orography. (Jarraud, M., A.J. Simmons and M. Kanamitsu; September 1986)

No.57 Zonal diagnostics of the ECMWF 1984-85 operational analyses and forecasts. (Brankovic, C.; October, 1986)

No.58 An evaluation of the performance of the ECMWF operational forecasting system in analysing and forecasting tropical easterly wave disturbances. Part 1: Synoptic investigation. (Reed, R.J., A. Hollingsworth, W.A. Heckley and F. Delsol; September, 1986)

No.59 Diabatic nonlinear normal mode initialisation for a spectral model with a hybrid vertical coordinate (Wergen, W.; December 1986).

No.60 An evaluation of the performance of the ECMWF operational forecasting system in analysing and forecasting tropical westerly wave disturbances. Part 2: Spectral investigation. (Reed, R.J., E. Klinker and A. Hollingsworth; September 1986).

No.61 Empirical orthogonal function analysis in the zonal and eddy components of 500 mb height fields in the Northern Extratropics (Molteni, F., January 1987).